1986ApJ...305..496H

THE ASTROPHYSICAL JOURNAL, 305:496–512, 1986 June 1
© 1986. The American Astronomical Society. All rights reserved. Printed in U.S.A.

ABSORPTION SPECTRUM OF THE $z = 3.78$ QSO 2000−330. I. THE LYMAN-ALPHA FOREST REGION AT 1.5 Å RESOLUTION

R. W. HUNSTEAD AND H. S. MURDOCH
School of Physics, University of Sydney

B. A. PETERSON
Mount Stromlo and Siding Spring Observatories

J. C. BLADES[1]
Space Telescope Science Institute

D. L. JAUNCEY AND A. E. WRIGHT
Division of Radiophysics, CSIRO

M. PETTINI
Royal Greenwich Observatory

AND

A. SAVAGE
Royal Observatory Edinburgh

Received 1985 June 12; accepted 1985 November 25

ABSTRACT

Spectra of the $z = 3.78$ QSO 2000−330 have been obtained at the Anglo-Australian Telescope with a resolution of ~1.5 Å FWHM. The region covered, 4100–5900 Å, extends from blueward of a continuum cutoff at 4150 Å to the red wing of Lyα. Structure in the profile of Lyα emission suggests the presence of Si III λ1206, the first time this line has been seen in emission in a QSO.

280 absorption lines are listed, and identifications are made in 45 Lyman-series systems and four heavy-element systems, the latter systems ranging in redshift from $z_{abs} = 3.1881$ to 3.5519. The $z_{abs} = 3.1881$ system is unusual in being purely low ionization, with no detectable Si IV or C IV. For this system we estimate $[O/H] \geq -1.1$ dex relative to solar, indicating an oxygen abundance at this early epoch that is surprisingly close to values typical of neutral interstellar clouds in the Galactic disk.

The mean density of Lyα absorption lines in 2000−330 has been compared with published values at lower redshift. We find a significant increase in line density (3.3 σ for $q_0 = 0$, 4.3 σ for $q_0 = \frac{1}{2}$) between $\langle z \rangle = 1.83$ and 3.41.

Subject headings: abundances — line identifications — quasars

I. INTRODUCTION

The QSO 2000−330 (≡PKS 2000−330) was identified on a UK Schmidt IIIa-J plate as a faint stellar object (Jauncey *et al.* 1982), which was subsequently found to have a redshift of 3.78 (Peterson *et al.* 1982). Its redshift remains the highest yet found, despite intensive searches for QSOs with $z > 3.5$ using objective prism techniques (e.g., Osmer 1983). The high luminosity of 2000−330 ($m_v = 17.3$ in the continuum) makes it an ideal candidate for intermediate- and high-resolution studies of its absorption spectrum. Of particular interest in this object are

i) the properties of the Lyα clouds at the highest redshifts yet observed, and

ii) the detection and properties of heavy-element absorption systems with $z_{abs} > 3$.

We present here spectral data at ~1.5 Å resolution covering the range 4100–5900 Å, i.e., from blueward of a continuum absorption cutoff at 4150 Å to the red wing of Lyα emission. As expected, the absorption spectrum of 2000−330 in this Lyα forest region is extraordinarily rich. Our main goals in this paper have been to establish first a continuum level and line list and then to carry out searches for heavy-element systems and Lyman-series systems. Existing techniques for identifying such systems had to be modified to cope with the high line density, on the one hand, and the limited wavelength coverage, on the other. Section II deals with the observing and reduction details, and § III covers the setting of continuum levels and the probable detection of Si III λ1206 in emission. The absorption line list is given in § IV, and the identification of many of the 280 lines is discussed in § V. A summary is given in § VI.

A brief discussion of Lyα line density evolution is included in § IV. A more detailed analysis is given in a separate paper (Murdoch *et al.* 1985, hereafter Paper II), where we combine the present data for 2000−330 with the substantial body of published data available at comparable resolution. We also examine in Paper II the global distribution of Lyα equivalent widths and the influence of spectral resolution on this distribution.

II. OBSERVATIONS AND PRELIMINARY REDUCTION

The observations of 2000−330 were obtained with the Image Photon Counting System (IPCS) mounted on the RGO spectrograph at the f/8 Cassegrain focus of the Anglo-Australian Telescope (AAT). The range 4100–5900 Å was covered in three spectra, which we label for convenience A, B and C; full details of the observations are listed in Table 1. The object was regularly beam-switched between two IPCS photocathode positions with the same total integration time in each

[1] Affiliated to the Astrophysics Division, Space Science Department of ESA.

© American Astronomical Society • Provided by the NASA Astrophysics Data System

1986ApJ...305..496H

TABLE 1

JOURNAL OF OBSERVATIONS OF 2000−330

Parameter	Spectrum A[a]	Spectrum B[b]	Spectrum C[b]
UT date	1982 Sep 15	1982 Sep 24	1982 Jul 15
Spectrograph camera focal length (cm)	25	82	82
Grating (grooves mm^{-1})	1200	600	600
Nominal dispersion (Å mm^{-1})	33	20	20
Wavelength range (Å)	4070–5010[c]	4825–5470	5365–5925
Slit width	1″.0	0″.7	0″.7
Seeing	1″.1	1″.0	1″.5
Measured resolution (Å, FWHM)	1.6	1.3	1.3
Integration time (minutes)	130	140	170
Mean continuum count[d]	140	150	65

[a] Observers Peterson, Jauncey, Wright, and Savage.
[b] Observers Hunstead, Murdoch, Blades, and Pettini.
[c] A short exposure made blueward of this region showed no measurable signal down to 3550 Å.
[d] Derived from the fitted continuum. Note that the instrumental response is comfortably oversampled by the detector. At the Nyquist sampling rate the mean counts become 200, 300 and 150 respectively.

position; individual integrations were typically 1000 s. The wavelength calibrations were established by frequent comparison spectra from a Cu-Ar hollow-cathode lamp. The data were flat-fielded using long tungsten-lamp exposures, and spectra B and C were flux-corrected using observations of the white dwarf standard L930-80 (Oke 1974).

The wavelength calibration of each spectrum was based on seventh-order polynomial fits to unblended argon lines giving rms residuals of typically 0.05 Å. The individual comparison spectra were then rebinned onto a linear wavelength scale and combined and smoothed in the same way as the object spectra. This composite arc spectrum was used to confirm the overall accuracy of the wavelength calibration and determine the variation in instrumental resolution along each spectrum. In each spectrum we found small systematic variations in resolution with wavelength, but these were confined to a range $\pm 10\%$ about the mean values quoted in Table 1.

In order to reduce the noise added to the object spectra by sky subtraction, the sky signal for each beam position was formed by using a much larger data window than that used for the object signal. By choosing a symmetrically expanded sky window and simple scaling, we retain good sky subtraction, provided the sensitivity variation along the slit is roughly linear. In practice, cancellation of the [O I] λ5577 night sky line in spectrum C is clearly adequate (see Fig. 4), considering that the peak line height is $\sim$20 times the estimated continuum level in 2000−330.

All data reduction was carried out at the AAO Epping laboratory using the SDRSYS reduction package.

III. CONTINUUM LEVELS

Before an absorption line list can be prepared, it is necessary to establish the level of the underlying continuum throughout the spectrum. The well-known problem in fitting a continuum to the region blueward of Lyα emission is particularly severe in 2000−330. The *direct* method of continuum estimation (Carswell *et al.* 1982) defines as continuum those regions where the local variance in the data is consistent with photon statistics. This method simply fails to locate enough line-free regions. The alternative *one-sided* method (Young *et al.* 1979) is also based on the local variance, but in this case the lowest points (which are presumed to occur in absorption lines) are progressively excluded until the variance is consistent with photon statistics. This method clearly relies on the local region containing some genuine continuum noise. Since there are so few regions in 2000−330 where the true continuum can be confidently recognized, the derived continuum levels would always be biased systematically low.

In view of the deficiencies inherent in these conventional methods for establishing continuum levels, we have adopted a more pragmatic approach based on reasonable assumptions about the form of the underlying continuum and taking advantage of the few regions of apparent continuum. The following constraints were imposed:

i) For spectra B and C, which had been flux-corrected, the underlying continuum was set to be a power law with constant exponent.

ii) In each spectrum the continuum fit was judged independently by three of us (R. W. H., H. S. M., B. A. P.), based on the requirement that positive excursions should be consistent with photon statistics. In the case of spectrum C, we took into account a higher resolution spectrum covering Lyα emission. The three continuum fits were very similar, and the adopted fit is a smoothed average. Of course, agreement among subjective estimates does not necessarily establish the estimates as correct.

iii) The preliminary continuum levels were examined in the regions of overlap between spectra A and B and between B and C, and minor adjustments were made to ensure consistency.

In regions of very high line density, placement of the continuum can be affected systematically by the amount of smoothing applied to the spectrum. Consequently, the trial fits were made on very lightly smoothed data. Despite this precaution, there remains the possibility that the sparse regions of apparent continuum are depressed by blends of weak lines or displaced by nonrandom fluctuations.

The adopted continuum levels in each spectrum are shown in Figure 1 superposed on the reduced spectra. Due to the cutoff in spectrum A, which corresponds to the Lyman limit in a heavy-element system at $z_{abs} = 3.5519$ (see § V), the true continuum cannot be defined below 4190 Å, and the adopted level was set arbitrarily to a constant value. In general, the continuum in spectrum A is more uncertain than the other two as a result of slightly lower resolution combined with an enhanced line density arising from higher order Lyman lines.

© American Astronomical Society • Provided by the NASA Astrophysics Data System

1986ApJ...305..496H

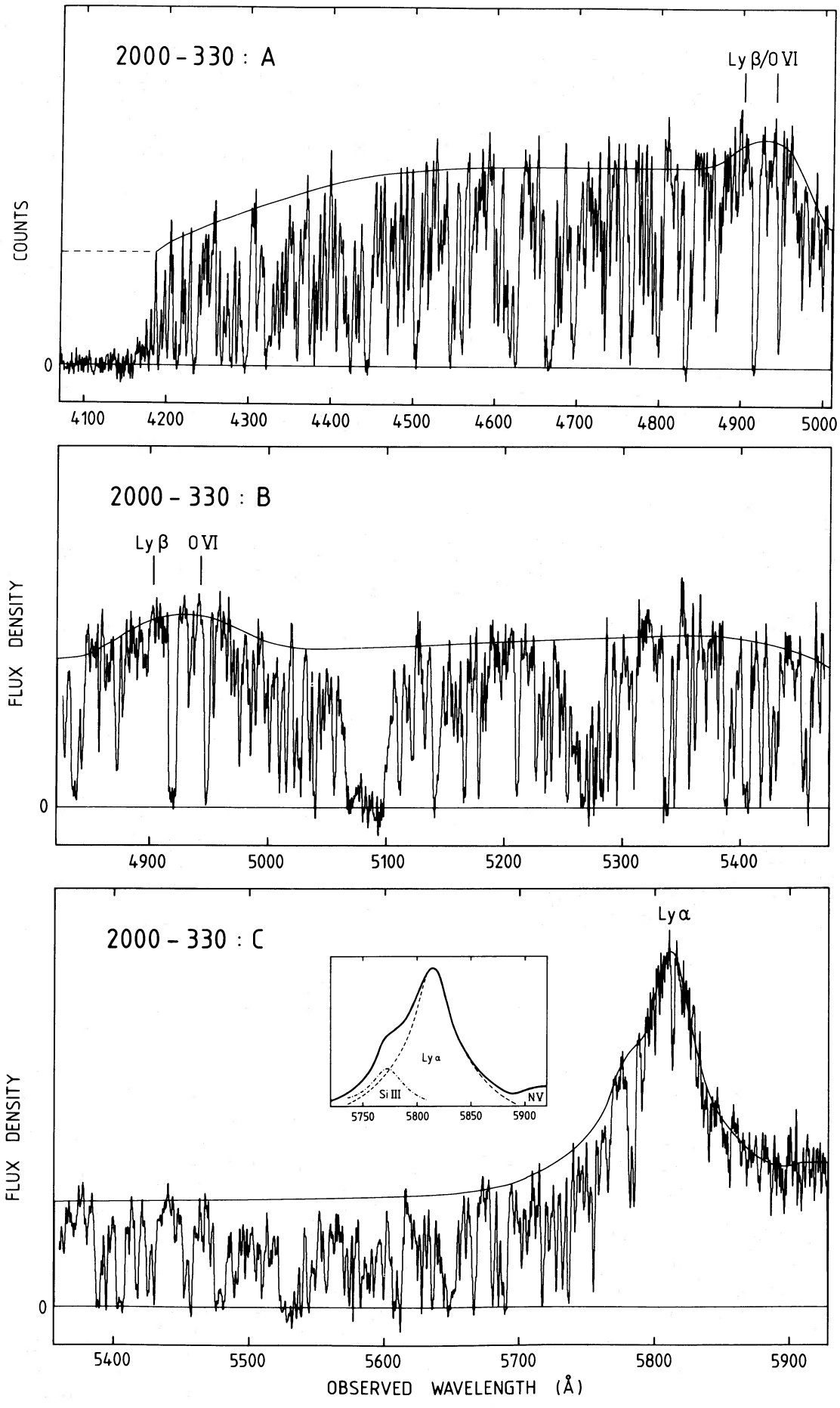

© American Astronomical Society • Provided by the NASA Astrophysics Data System

1986ApJ...305..496H

TABLE 2

EMISSION LINE PARAMETERS

Line	λ_{obs} (Å)	z_{em}	FWHM (Å)
Lyα λ1215	5814	3.783	45
Si III λ1206	5773	3.785	35:

Recent data at higher resolution (obtained by R. W. H., H. S. M., J. C. B., and M. P.), covering selected portions of the Lyman forest region, have generally supported the levels shown in Figure 1.

Emission lines.—In attempting to define the continuum around the Lyα emission line, it was noticed that the line appeared markedly asymmetric. This was initially thought to be due to Lyα absorption in the blue wing, as suggested by Peterson *et al.* (1982). However, the high-resolution AAT spectrum referred to above showed no sign of narrow clustered absorption lines, such as would have been required to explain the observed asymmetry. We therefore explored the possibility that an additional emission line was contributing to the observed profile.

After defining regions in the emission profile which appeared free of absorption, we fitted a smooth (but otherwise unconstrained) curve through the data. The red wing of the line (after compensation for slight contamination by the well-separated N V λ1240 emission) was reflected about the peak and subtracted from the blue wing. The residue could plausibly be explained by an additional emission line, and its rest wavelength immediately identified it as Si III λ1206. The deconvolution of the Lyα profile is shown as an inset in the bottom panel of Figure 1. The emission line parameters are listed in Table 2.

If this interpretation is correct, this would be the first detection of Si III emission in a QSO. The narrowness of Lyα (FWHM $\approx$ 2300 km s^{-1}) has clearly facilitated the detection in 2000−330, and we would encourage a search for Si III in other narrow-line QSOs.

The N V λ1240 line is only partly included in spectrum C; although no useful quantitative measures are possible, it appears to be roughly of the same strength as the newly discovered Si III line. Using the improved redshift estimates obtained above, we were able to confirm that both Lyβ and O VI λ1034 contribute to the low-profile emission line near 4935 Å.

IV. ABSORPTION LINE LIST

After continuum fitting, each spectrum was normalized by dividing by the fitted continuum. Due to the extreme blending problems over the entire spectral range, it was not practicable to use an automated procedure for selecting absorption lines. For some lines the boundaries could be defined by continuum crossings. Otherwise, the boundaries between lines were set at local maxima, following the method used by Carswell *et al.* (1982). For measuring line centroids and equivalent widths, the boundaries were assumed to extend up to the adopted continuum level.

In setting line boundaries we have looked for clear evidence of separate lines based on Poisson noise statistics. In general, features with broad or asymmetric profiles have been counted as single lines. Noise fluctuations below the zero level in strong, saturated lines were a useful guide to the plausibility of small fluctuations above the zero level. Positive fluctuations in the rare sections of true continuum were also helpful in gauging the reality of weak absorption lines. The line assignments could be made with greater confidence in the regions of overlap between adjacent spectra.

These methods for selecting lines and measuring their parameters are well defined and repeatable. We believe that they yield a Lyα sample which is directly comparable with existing samples at lower redshift (e.g., Young, Sargent, and Boksenberg 1982). More sophisticated methods, such as Voigt profile fitting, are not justified and have not generally been used at this resolution.

The full line list is given in Table 3. The centroid wavelengths and equivalent widths have been rounded to 0.1 Å to reflect the uncertainties in the placement of line boundaries and continuum. A comparison between lines in the overlapping regions indicates that rms uncertainties are $\sim$0.2 Å in both λ_{obs} and W_{obs} for narrow, unsaturated lines. Some of the lines with $W_{obs} \leq 0.6$ Å may therefore be spurious, and the list will not be complete at this level due to blending. On the other hand, we expect the line list to be highly reliable and essentially complete for $W_{obs} \geq 1.0$ Å. For stronger lines the continuum uncertainties ($\gtrsim$10%) will dominate the error in W_{obs}.

The line identifications listed in Table 3 were made after a thorough search for Lyman-series and heavy-element absorption systems. Further details are given in the footnotes, and the techniques are described in § V. The final column of the table indicates the spectrum from which the quoted measures were obtained. In the case of overlapping spectra, the choice was based on the best combination of signal-to-noise ratio and spectral resolution.

Expanded plots of spectra A, B, and C are given in Figures 2, 3, and 4 respectively. These spectra have been divided by the adopted continuum levels shown in Figure 1, and the absorption lines listed in Table 3 are marked.

It is interesting to compare the mean density of Lyα absorption lines in 2000−330 with the corresponding values obtained by Young, Sargent, and Boksenberg (1982) at lower redshift. Adopting their selection criteria, we find a total of 76 Lyα lines between Lyβ and Lyα emission with rest equivalent width 0.32 Å or greater; these lines are marked with an asterisk in the final column of Table 3. The corresponding density of lines per unit redshift is 102 $\pm$ 12 at a mean redshift $\langle z \rangle = 3.41$. Normalized for cosmological effects, the density becomes 23.1 $\pm$ 2.6 for $q_0 = 0$ or 48.4 $\pm$ 5.6 for $q_0 = \frac{1}{2}$. Young *et al.* obtained normalized densities of 11.7 $\pm$ 2.2 ($q_0 = 0$) and 19.6 $\pm$ 3.7 ($q_0 = \frac{1}{2}$) for a sample with $\langle z \rangle = 1.83$. The difference between these line densities is 3.3 σ for $q_0 = 0$ and 4.3 σ for $q_0 = \frac{1}{2}$, showing clear evidence for evolution in the Lyα line density over this redshift interval. Peterson (1983*a*, *b*) reached a similar conclusion based on a larger sample of QSOs which included the data from spectrum C of 2000−330.

A detailed discussion of the line density evolution is given in Paper II.

FIG. 1.—Adopted continuum fits for the three spectra of 2000−330. The ordinate is net photon counts for the top panel (spectrum A) and flux density f_ν on an arbitrary scale for the lower two panels. The expected positions of Lyβ λ1025 and O VI λ1034 emission are indicated. Differences in appearance between the red end of spectrum A and the blue end of B are a consequence of the lower dispersion and lack of flux calibration for the former. At the blue end of A, where the true continuum level cannot be defined, we adopt a constant level solely for the purpose of continuum division. (*inset*) Deconvolution of the Lyα emission profile showing the presence of Si III λ1206. The underlying continuum has been subtracted.

© American Astronomical Society • Provided by the NASA Astrophysics Data System

TABLE 3

ABSORPTION LINE LIST FOR 2000 – 330

Line no.	λ_{obs} (Å)	W_{obs} (Å)	Line identification	Spectrum
1	4191.7	5.0	Incl H I(920),z=3.5519	A
2	4196.5	2.5		A
3	4201.9	3.7	H I(923),z=3.5519	A
4	4210.5	3.2	Incl H I(949),z=3.4333	A
5	4215.6	6.0	H I(972),z=3.3332; H I(926),z=3.5519	A
6	4221.7	1.6	H I(972),z=3.3406	A
7	4225.9	3.8	Incl H I(1025),z=3.1215	A
8	4235.2	8.2	Incl H I(1025),z=3.1261+3.1320; H I(930),z=3.5519	A
9	4242.3	1.6		A
10	4245.9	0.9		A
11	4249.8	0.7		A
12	4253.6	2.1	H I(1025),z=3.1463	A
13	4262.8	3.5		A
14	4268.4	4.2	H I(937),z=3.5519	A
15	4272.9	3.1		A
16	4279.6	6.4	H I(1025),z=3.1723(trough)	A
17	4286.8	3.6	H I(1025),z=3.1793(trough)	A
18	4296.5	10.8	H I(1025),z=3.1881+3.1914(trough)	A
19	4312.1	3.7	H I(972),z=3.4333; H I(1025),z=3.2048	A
20	4317.7	1.0		A
21	4325.1	9.6	H I(972),z=3.4471; H I(949),z=3.5519	A
22	4333.5	3.2		A
23	4338.9	3.6	H I(1025),z=3.2303; C II(1036),z=3.1881	A
24	4343.5	2.3	C II(1036),z=3.1914	A
25	4347.7	1.9		A
26	4352.4	0.9	O I(1039),z=3.1881	A
27	4357.2	2.4	H I(930),z=3.6813; O I(1039),z=3.1914	A
28	4361.2	3.4	H I(1025),z=3.2502; H I(972),z=3.4859	A
29	4366.2	1.6	H I(972),z=3.4898	A
30	4369.7	0.6	H I(1025),z=3.2603	A
31	4376.9	4.5		A
32	4382.2	2.6	H I(972),z=3.5059	A
33	4385.5	2.2	H I(949),z=3.6173; H I(972),z=3.5099	A
34	4390.1	2.5	H I(937),z=3.6813	A
35	4396.6	3.0	Incl H I(1025),z=3.2872	A
36	4403.8	1.4	H I(949),z=3.6369	A
37	4409.0	3.3		A
38	4414.0	1.2	H I(949),z=3.6476	A
39	4417.9	2.5	H I(1025),z=3.3073	A
40	4421.7	2.7		A
41	4426.4	5.4	H I(972),z=3.5519	A
42	4432.6	2.9	H I(972),z=3.5575; H I(1025),z=3.3223	A
43	4436.4	2.5	Incl H I(972),z=3.5619	A
44	4445.8	10.0	Incl H I(949),z=3.6813; H I(1025),z=3.3332	A
45	4452.8	1.3	H I(1025),z=3.3406	A
46	4458.4	1.8	H I(1025),z=3.3466	A
47	4463.3	1.5		A
48	4470.8	4.2	Incl H I(1025),z=3.3569; may incl O VI(1031),z=3.3332	A
49	4476.4	1.6		A
50	4482.5	3.2	Incl H I(1025),z=3.3684 in blue wing	A
51	4487.5	0.7	H I(972),z=3.6139	A
52	4490.5	1.7	H I(972),z=3.6173; C II(1036),z=3.3332	A
53	4496.2	2.3	May incl O VI(1037),z=3.3332	A
54	4503.4	2.9	H I(1025),z=3.3913; O I(1039),z=3.3332	A
55	4506.4	2.9	Si II(989),z=3.5519	A
56	4509.5	2.2	H I(972),z=3.6369	A
57	4513.5	1.4		A
58	4519.9	1.6	H I(972),z=3.6476	A
59	4523.0	1.2	H I(972),z=3.6507	A
60	4527.1	0.5		A
61	4533.0	1.4		A
62	4536.7	1.5		A
63	4540.1	0.7	N II(1083),z=3.1881	A
64	4547.5	5.8	H I(1025),z=3.4333; N II(1083),z=3.1914 in blue wing	A
65	4552.8	2.8	H I(972),z=3.6813	A
66	4561.6	5.0	H I(1025),z=3.4471	A
67	4572.1	3.3		A
68	4579.1	1.0	H I(1025),z=3.4640	A
69	4582.9	0.5		A
70	4590.2	0.9	H I(972),z=3.7203	A
71	4601.2	1.8	H I(1025),z=3.4859	A
72	4606.0	3.5	Incl H I(1025),z=3.4898	A
73	4613.1	1.8		A
74	4615.7	1.7		A
75	4620.6	5.5	Incl H I(1025),z=3.5059	A
76	4627.9	6.5	Incl H I(1025),z=3.5099	A
77	4634.8	0.7		A
78	4645.4	0.9	H I(1025),z=3.5291	A
79	4650.0	1.7	H I(1025),z=3.5337	A
80	4657.2	1.6		A
81	4663.7	3.4		A
82	4669.3	7.4	H I(1025),z=3.5519	A
83	4674.6	2.3	H I(1025),z=3.5575	A
84	4679.2	1.9	H I(1025),z=3.5619	A
85	4683.0	2.7		A
86	4690.3	1.5	H I(1025),z=3.5727	A
87	4698.2	6.6		A
88	4704.6	1.4	H I(1025),z=3.5866	A
89	4710.9	2.0	Incl H I(1025),z=3.5933	A
90	4717.5	0.7	C II(1036),z=3.5519	A
91	4721.6	1.2		A
92	4725.8	1.1	H I(1025),z=3.6072	A
93	4730.1	0.5	O I(1039),z=3.5519	A
94	4732.5	1.6	H I(1025),z=3.6139	A
95	4736.1	2.2	H I(1025),z=3.6173	A
96	4741.9	1.1		A
97	4749.5	0.6	H I(1025),z=3.6304	A
98	4755.6	3.6	H I(1025),z=3.6369; N I(1134),z=3.1914	A
99	4763.3	0.7		A
100	4767.2	3.8	H I(1025),z=3.6476	A

© American Astronomical Society • Provided by the NASA Astrophysics Data System

TABLE 3—*Continued*

Line no.	λ_{obs} (Å)	W_{obs} (Å)	Line identification	Spectrum
101	4770.4	1.4	H I(1025), z=3.6507	A
102	4778.0	1.0		A
103	4782.7	1.8	H I(1025), z=3.6625	A
104	4788.6	1.7		A
105	4794.5	2.5	H I(1025), z=3.6740; Fe II(1144), z=3.1881	A
106	4800.5	5.1	H I(1025), z=3.6813; Fe II(1144), z=3.1914	A
107	4805.6	1.6		A
108	4818.3	0.7		A
109	4825.9	2.2	H I(1025), z=3.7046	A
110	4835.7	7.5		A
111	4842.0	2.2	H I(1025), z=3.7203	A
112	4857.0	0.9	H I(1025), z=3.7352	B
113	4862.3	0.5		B
114	4865.0	0.5	Fe III(1122), z=3.3332	B
115	4872.3	3.0		B
116	4877.5	1.1		B
117	4882.0	0.4		B
118	4889.0	0.7		B
119	4896.5	1.3		B
120	4919.5	7.0		B*
121	4933.3	1.2		B
122	4937.6	0.4		B
123	4948.2	4.4		B*
124	4954.1	0.8		B
125	4964.8	0.5		B
126	4969.1	0.6		B
127	4972.2	0.8		B
128	4976.3	2.1		B*
129	4983.3	0.8		B
130	4985.6	1.3	Si II(1190), z=3.1881	B
131	4989.6	1.1	Si II(1190), z=3.1914	B
132	4997.9	1.4	Si II(1193), z=3.1881	B
133	5001.7	1.8	Si II(1193), z=3.1914	B
134	5005.3	0.9		B
135	5010.4	2.8	H I(1215), z=3.1215	B*
136	5016.0	2.7	H I(1215), z=3.1261	B*
137	5023.2	2.2	H I(1215), z=3.1320	B*
138	5026.4	1.7	May incl N I(1199), z=3.1881	B
139	5028.7	1.9	Incl N I(1199), z=3.1914	B
140	5035.7	2.2		B*
141	5040.5	4.0	H I(1215), z=3.1463	B*
142	5045.4	1.2		B
143	5048.1	1.1		B
144	5052.1	1.0	Prob Si III(1206), z=3.1881	B
145	5056.8	3.3	Si III(1206), z=3.1914	B
146	5084.2	39.4	H I(1215), z=3.16 - 3.20 (trough)	B*
147	5111.7	4.4	H I(1215), z=3.2048	B*
148	5118.0	1.3		B
149	5122.4	2.6		B*
150	5133.1	2.1		B*
151	5143.0	7.2	H I(1215), z=3.2303	B*
152	5151.0	1.5		B*
153	5155.6	0.6		B
154	5157.9	1.2	Incl Si II(1190), z=3.3332	B
155	5161.3	1.6		B*
156	5166.8	3.9	H I(1215), z=3.2502	B*
157	5170.6	0.3	Si II(1193), z=3.3332	B
158	5173.8	0.9		B
159	5179.3	2.6	H I(1215), z=3.2603	B*
160	5182.6	0.9		B
161	5185.3	0.9		B
162	5197.8	0.6		B
163	5211.8	3.6	H I(1215), z=3.2872; Fe II(1144), z=3.5519	B
164	5221.1	0.7		B
165	5228.1	2.5	Si III(1206), z=3.3332	B
166	5232.2	1.6		B*
167	5236.4	2.9	H I(1215), z=3.3073	B*
168	5240.8	1.8		B*
169	5245.4	0.5		B
170	5248.0	1.0		B
171	5250.4	1.1		B
172	5254.5	3.3	H I(1215), z=3.3223	B*
173	5259.8	3.8		B*
174	5263.6	1.6		B*
175	5267.8	5.0	H I(1215), z=3.3332	B*
176	5272.7	3.2		B*
177	5276.7	2.1	H I(1215), z=3.3406	B*
178	5279.1	1.6	Si II(1260), z=3.1881	B
179	5283.5	4.1	H I(1215), z=3.3466; Si II(1260), z=3.1914	B
180	5288.9	1.5		B*
181	5290.9	1.2		B
182	5296.6	2.3	H I(1215), z=3.3569	B*
183	5303.2	0.5		B
184	5306.5	1.1		B
185	5310.5	2.3	H I(1215), z=3.3684	B*
186	5338.4	6.2	H I(1215), z=3.3913	B*
187	5345.1	2.4		B*
188	5357.6	1.9		B*
189	5362.5	1.6		B*
190	5371.6	1.0		B
191	5381.6	0.9		B
192	5389.1	4.7	H I(1215), z=3.4333	B*
193	5392.4	0.8		B
194	5395.5	2.3		B*
195	5399.1	0.6		B
196	5406.0	6.7	H I(1215), z=3.4471	B*
197	5411.5	0.8		B
198	5418.4	3.1	Si II(1190), z=3.5519	B
199	5426.4	3.2	H I(1215), z=3.4640	B*
200	5431.3	2.9	Si II(1193), z=3.5519	B

© American Astronomical Society • Provided by the NASA Astrophysics Data System

TABLE 3—*Continued*

Line no.	λ_{obs} (Å)	W_{obs} (Å)	Line identification	Spectrum
201	5436.9	0.7		B
202	5446.9	0.9		C
203	5453.6	3.5	H I(1215),z=3.4859; O I(1302),z=3.1881	C
204	5458.2	3.6	H I(1215),z=3.4898; O I(1302),z=3.1914	C
205	5462.6	1.1	Si II(1304),z=3.1881; Si II(1260),z=3.3332	C
206	5466.9	1.0	Si II(1304),z=3.1914	C
207	5472.7	1.3		C
208	5477.6	4.7	H I(1215),z=3.5059	C*
209	5482.6	4.9	H I(1215),z=3.5099	C*
210	5486.9	0.7		C
211	5489.9	2.5		C*
212	5492.7	2.0	Si III(1206),z=3.5519	C
213	5495.6	0.9		C
214	5498.4	1.4		C
215	5501.5	1.5		C*
216	5506.0	2.1	H I(1215),z=3.5291	C*
217	5508.3	0.7		C
218	5511.5	3.2	H I(1215),z=3.5337	C*
219	5516.4	1.5		C*
220	5518.6	1.0		C
221	5521.4	1.2		C
222	5530.8	15.6	H I(1215),z=3.5519	C*
223	5540.4	3.1	H I(1215),z=3.5575	C*
224	5545.7	4.0	H I(1215),z=3.5619	C*
225	5550.4	3.0	Line may be double	C*
226	5555.2	0.9		C
227	5558.8	3.3	H I(1215),z=3.5727	C*
228	5564.0	1.5		C*
229	5566.7	0.4		C
230	5569.2	1.0		C
231	5572.2	2.1		C*
232	5575.7	2.5	H I(1215),z=3.5866	C*
233	5579.2	2.3:	Affected by night sky [O I](5577)	C*
234	5584.5	3.4	Incl H I(1215),z=3.5933; line probably double	C*
235	5588.6	2.1	C II(1334),z=3.1881	C
236	5590.7	1.6		C*
237	5593.7	2.3	C II(1334),z=3.1914	C
238	5596.5	1.3	Uncertain line, no clear minimum	C
239	5600.7	2.9	H I(1215),z=3.6072	C*
240	5605.5	1.5		C*
241	5608.9	3.8	H I(1215),z=3.6139	C*
242	5613.2	4.2	H I(1215),z=3.6173	C*
243	5622.0	0.8		C
244	5625.6	1.8		C*
245	5629.1	2.2	H I(1215),z=3.6304	C*
246	5632.6	1.3		C
247	5637.0	3.5	H I(1215),z=3.6369	C*
248	5640.8	1.0		C
249	5642.9	1.1	O I(1302),z=3.3332	C
250	5645.3	2.2		C*
251	5650.8	8.0	H I(1215),z=3.6476+3.6507; poss Si II(1304),z=3.3332	C*
252	5657.5	1.5		C*
253	5661.8	1.0		C
254	5667.8	4.3	H I(1215),z=3.6625	C*
255	5681.8	2.9	H I(1215),z=3.6740	C*
256	5686.1	1.9		C*
257	5690.8	5.1	H I(1215),z=3.6813	C*
258	5697.8	0.7		C
259	5701.0	0.9		C
260	5703.5	1.4		C
261	5707.5	1.9		C*
262	5714.0	1.0		C
263	5719.0	2.9	H I(1215),z=3.7046	C*
264	5724.0	2.2		C*
265	5729.1	2.3		C*
266	5734.0	2.6		C*
267	5738.4	2.8	H I(1215),z=3.7203; Si II(1260),z=3.5519	C
268	5743.2	1.1		C
269	5746.8	0.6		C
270	5749.6	0.8		C
271	5753.0	1.1		C
272	5756.4	2.1	H I(1215),z=3.7352	C*
273	5760.6	1.0		C
274	5767.1	1.3		C
275	5782.7	1.7	C II(1334),z=3.3332	C
276	5786.0	1.6		C*
277	5792.2	0.6		C
278	5814.7	0.7		C
279	5841.6	0.5	Si IV(1393),z=3.1914	C
280	5857.0	0.5		C

NOTES.—All wavelengths are vacuum, heliocentric values.

"Incl" indicates that the listed identification(s) is included in the line but is unlikely to account for the entire observed equivalent width. Multiple assignments are based on other information such as superposed plots; see text.

Redshifts given for line identifications are adopted system values; individual line redshifts are given in Tables 4 and 6.

* Counted as H I λ1215 lines in Paper II; these lines have rest equivalent width $W \geq 0.32$ Å.

© American Astronomical Society • Provided by the NASA Astrophysics Data System

1986ApJ...305..496H

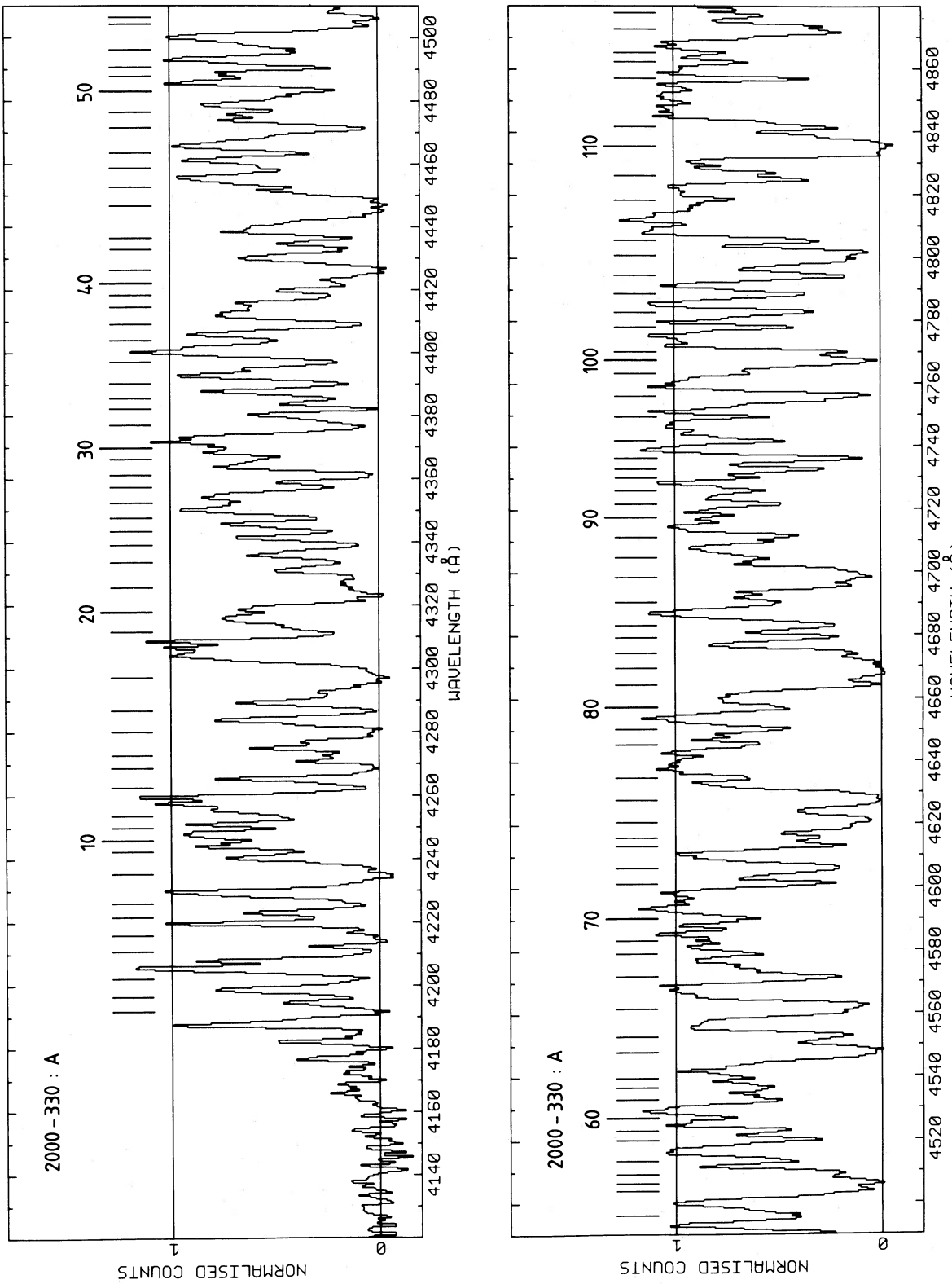

FIG. 2.—Spectrum A, normalized by dividing by the adopted continuum shown in Fig. 1. The absorption lines are marked and labeled.

© American Astronomical Society • Provided by the NASA Astrophysics Data System

1986ApJ...305..496H

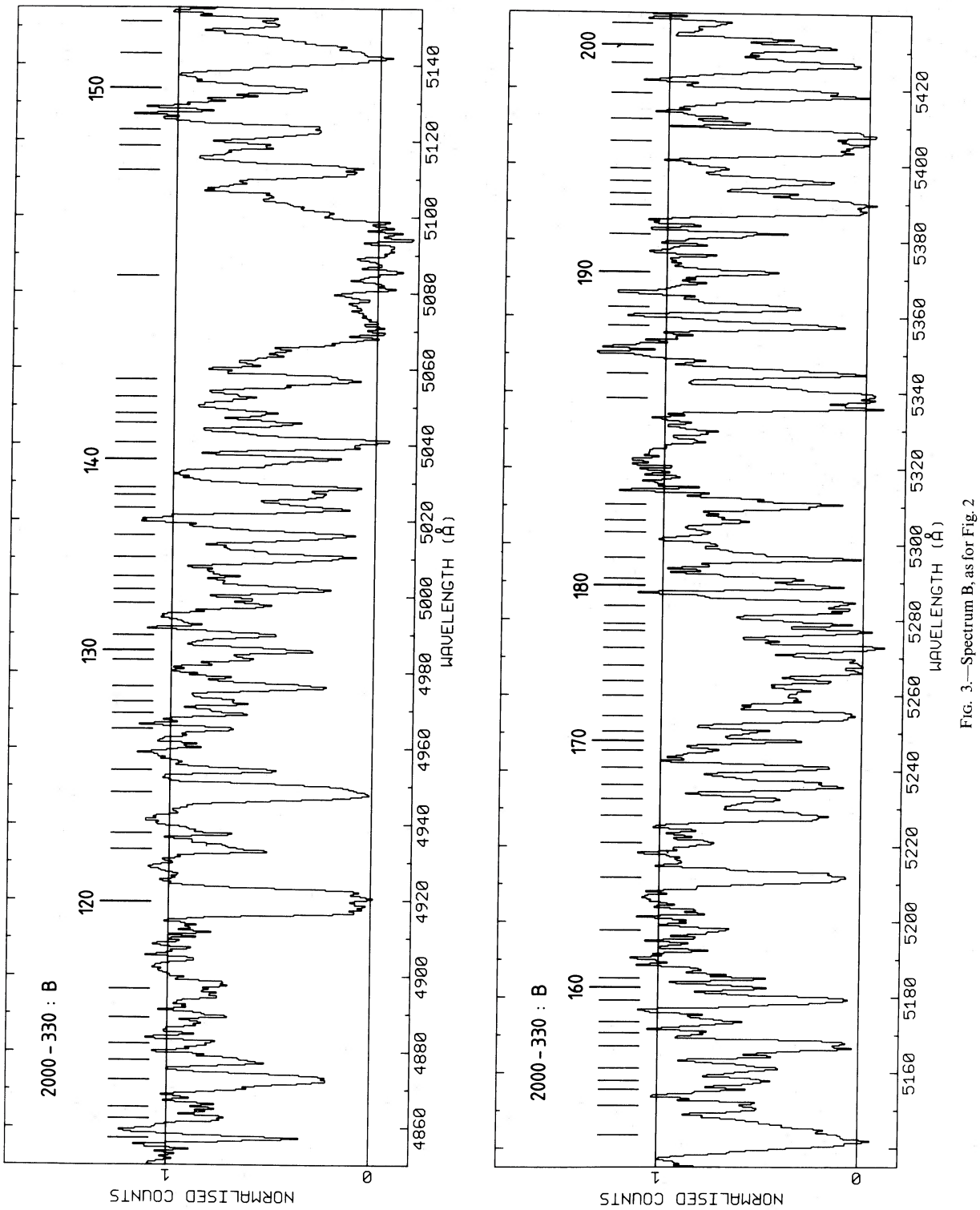

FIG. 3.—Spectrum B, as for Fig. 2

© American Astronomical Society • Provided by the NASA Astrophysics Data System

1986ApJ...305..496H

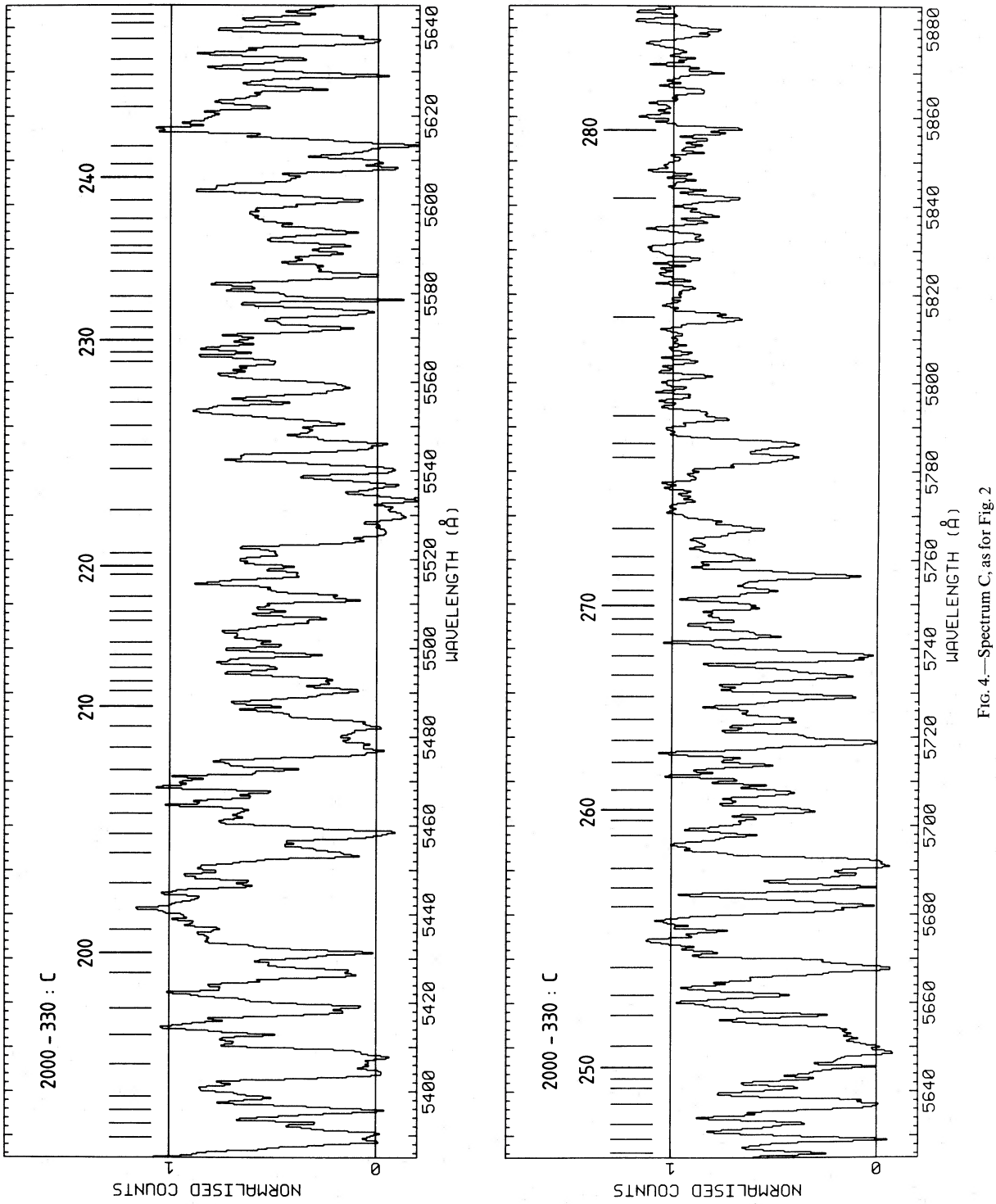

FIG. 4.—Spectrum C, as for Fig. 2

© American Astronomical Society • Provided by the NASA Astrophysics Data System

1986ApJ...305..496H

V. ABSORPTION LINE SYSTEMS

a) Lyman-Series Systems

The very high density of lines in 2000−330 makes it difficult to conduct a reliable automated search for Lyman-line systems. Instead, our search method made use of superposed spectrum plots prepared according to the scheme outlined below:

We first note that the Lyman continuum cutoff at ∼4190 Å defines the lower limit for Lyβ (and therefore for a claimable Lyman system) at $z_{abs} = 3.08$. The corresponding lower limit for Lyγ is at $z_{abs} = 3.31$, for Lyδ is at $z_{abs} = 3.41$, and so on.

Over the range $3.10 < z_{abs} < 3.78$, the normalized spectra were rebinned onto logarithmic wavelength scales with 15 km s^{-1} per channel and origins set to correspond with Lyα, Lyβ, etc. These spectra were plotted directly on top of one another, using different colors.

Correspondences between Lyα, Lyβ, etc., were easy to locate on the superposed plots and alignments between putative Lyman-series lines could be examined in detail. In particular, we looked for both a plausible decrement in equivalent width and a plausible profile match. These requirements were relaxed only when there was clear evidence of blending.

Using this method we have identified 45 Lyman systems, which are listed in Table 4. Individual line redshifts and rest equivalent widths are given. In general, our emphasis has been on reliability rather than completeness. The reliability of the systems is clearly a function of the number of Lyman lines actually identified. This in turn depends on the column density of neutral hydrogen *and* on the redshift. Conflicts in the assignment of individual lines could generally be resolved by the superposed plots.

The majority of Lyman absorption systems seem to have decrements in equivalent width (from Lyα to higher order lines) which place the absorbing clouds on the saturated part of the curve of growth. Nevertheless, for many systems we were able to obtain useful values of velocity dispersion b and column density N, based on the unblended lines in Table 4 and assuming a single cloud model. In cases where *all* the lines fall on the saturated part of the curve of growth a considerable range of solutions is possible, and we have opted for the larger b/lower N solution.

Values of log N(cm^{-2}) range from 14.3 to 16.5, with b from 30 to 70 km s^{-1}. Our instrumental resolution corresponds to a b value of ∼40 km s^{-1}. At higher resolution ($b \approx 12$ km s^{-1}), Carswell *et al.* (1984) found that Lyα lines in 1101−264 had b values in the range 10–45 km s^{-1}. It therefore seems likely that some of the Lyα lines in Table 4 will turn out to be multiple.

b) Heavy-Element Systems

Searches for heavy-element absorption systems usually rely heavily on lines redward of Lyα emission, where the spectrum is relatively uncrowded. The present data for 2000−330 extended only up to the Lyα emission line, so we were faced with extreme problems arising from blending. However, even within the Lyα forest alone we have identified four definite heavy-element systems using the stringent procedures described below. These systems have subsequently been confirmed by more recent spectra obtained redward of Lyα (Hunstead *et al.* 1986).

Our basic search method followed that used previously by Bahcall (1968), Young *et al.* (1979), and others. A search list of metal lines was redshifted and cross-correlated with the line list in Table 3. The fraction of successful matches in wavelength was then plotted as a function of redshift; the acceptance window for a wavelength match was set to ±1 Å, and the redshift step size was $\Delta z = 0.0005$. The following additional constraints were found necessary:

1. In order to reduce the rate of spurious correlations we restricted the initial search list to the 11 lines listed in Table 5A. H I was not included at this stage, because it was found that the large number of Lyman-only systems adds noise to the cross-correlation.
2. Following tests, the range of redshift searched was set at $z_{abs} = 3.1$–3.78. In this range, Lyα in a potential heavy-element system cannot be confused with other Lyman series lines, and Lyβ is accessible above the continuum cutoff.

Cross-correlation peaks which appeared significant in comparison with the noise were examined more closely after calling on the additional lines listed in Table 5B. The line assignments were then checked for plausibility. This filtering process was effective in rejecting most of the "systems," usually because of implausible relative strengths among transitions in a particular ion or the absence of Lyα.

This procedure led to the detection of four well-defined heavy-element systems. In Table 6 we present the line identifications in these systems and include mention of key lines which were not detected. Rest wavelengths λ_0 and oscillator strengths f are taken from Morton (1978).

A final check of the line identifications was made using superposed plots, as described in § V*a* for the Lyman-series systems. This direct profile comparison among different species (or different transitions in the one species) allows a more reliable assessment of identifications and blends than is possible in conventional cross-correlation searches based solely on line centroids. Discussion of specific identifications and of the overall properties of the systems is given below.

i) $z_{abs} = 3.1881$ *and* 3.1914

These systems are analyzed together because they are very close in redshift and are blended in Lyα and Lyβ. The Lyα lines lie near the red edge of the broad Lyα trough spanning 5060–5105 Å (Fig. 3, line 146). The redshift difference, interpreted as a velocity difference, is 240 km s^{-1}. If the two systems arise in intervening galaxies, such a velocity difference is plausible for two galaxies in a group or cluster.

Both systems show strong low-ionization lines typical of sightlines through the interstellar medium in the disk of our Galaxy, but only the $z_{abs} = 3.1914$ system shows Si IV (and also C IV; Hunstead *et al.* 1986), which in our Galaxy occurs predominantly in the halo. Even Si III λ1206 is weak at $z_{abs} = 3.1881$, and its identification is by no means secure. This system is, therefore, unusual among QSO absorption systems in being exclusively a low-ionization system. Moreover, a search strategy which was weighted toward the C IV and Si IV doublets would probably have missed this system altogether.

Practically all the neutrals and single ions in Table 5 are detected in these systems. There is uncertainty, however, regarding N I $\lambda\lambda$1134, 1199, since each "line" is in fact triple and there is some overlap between the two systems. Higher resolution data are needed to confirm the tentative identifications in Table 6.

A superposed plot of several species in these systems is shown in Figure 5 to illustrate the need for examining line

© American Astronomical Society • Provided by the NASA Astrophysics Data System

TABLE 4

LYMAN SERIES ABSORPTION SYSTEMS IN 2000 – 300

Adopted redshift	b (km s^{-1})	log N (cm^{-2})	Ident.	Line no.	z_{abs}	W (Å)	Notes*
3.7352	35	14.6	H I(1215)	272	3.7352	0.44	
			H I(1025)	112	3.7352	0.19	
3.7203			H I(1215)	267	3.7204	0.59	1
			H I(1025	111	3.7206	0.47	2
			H I(972)	70	3.7198	0.19	2
3.7046			H I(1215)	263	3.7044	0.62	
			H I(1025)	109	3.7049	0.47	2
3.6813	50	16.5	H I(1215)	257	3.6812	1.09	
			H I(1025)	106	3.6801	1.09	1
			H I(972)	65	3.6814	0.60	
			H I(949)	44	(3.6811	2.14)	3
			H I(937)	34	3.6813	0.53	
			H I(930)	27	3.6814	0.51	1
3.6740			H I(1215)	255	3.6738	0.62	
			H I(1025)	105	3.6743	0.53	1
3.6625	70	14.9	H I(1215)	254	3.6623	0.92	4
			H I(1025)	103	3.6628	0.39	
3.6507			H I(1215)	251	(3.6483	1.72)	5
			H I(1025)	101	3.6508	0.30	
			H I(972)	59	3.6507	0.26	
3.6476	100:	15.2:	H I(1215)	251	(3.6483	1.72)	5
			H I(1025)	100	3.6477	0.82	
			H I(972)	58	3.6475	0.34	
			H I(949)	38	3.6476	0.26	2
3.6369	40:	15.8:	H I(1215)	247	3.6369	0.75	
			H I(1025)	98	3.6364	0.78	2
			H I(972)	56	3.6368	0.47	
			H I(949)	36	3.6369	0.30	
3.6304	50	14.3	H I(1215)	245	3.6305	0.48	
			H I(1025)	97	3.6304	0.13	
3.6173	60	15.2	H I(1215)	242	3.6174	0.91	
			H I(1025)	95	3.6173	0.48	
			H I(972)	52	3.6173	0.37	1
			H I(949)	33	3.6176	0.48	2
3.6139	60	14.9	H I(1215)	241	3.6138	0.82	
			H I(1025)	94	3.6138	0.35	
			H I(972)	51	3.6142	0.15	
3.6072	50	14.7	H I(1215)	239	3.6071	0.63	
			H I(1025)	92	3.6073	0.24	
3.5933:			H I(1215)	234	3.5938	0.74	2
			H I(1025)	89	3.5928	0.44	2
3.5866	35	15.0	H I(1215)	232	3.5865	0.55	
			H I(1025)	88	3.5866	0.31	
3.5727	50	14.9	H I(1215)	227	3.5726	0.72	4
			H I(1025)	86	3.5727	0.33	4
3.5619	60	15.0	H I(1215)	224	3.5619	0.88	
			H I(1025)	84	3.5619	0.42	
			H I(972)	43	3.5617	0.55	2
3.5575			H I(1215)	223	3.5575	0.68	
			H I(1025)	83	3.5574	0.50	
			H I(972)	42	3.5578	0.64	2
3.5337	50	15.0	H I(1215)	218	3.5337	0.71	
			H I(1025)	79	3.5334	0.37	
3.5291	35	14.6	H I(1215)	216	3.5292	0.46	
			H I(1025)	78	3.5289	0.20	
3.5099			H I(1215)	209	3.5099	1.09	
			H I(1025)	76	(3.5119	1.44)	3
			H I(972)	33	3.5093	0.49	2
3.5059	50	16.0	H I(1215)	208	3.5058	1.04	
			H I(1025)	75	(3.5047	1.22)	4
			H I(972)	32	3.5059	0.57	
3.4898			H I(1215)	204	3.4899	0.80	1
			H I(1025)	72	3.4905	0.78	2
			H I(972)	29	3.4895	0.36	
3.4859			H I(1215)	203	3.4861	0.78	1
			H I(1025)	71	3.4858	0.40	
			H I(972)	28	(3.4843	0.76)	3
3.4640	70	14.5	H I(1215)	199	3.4637	0.72	
			H I(1025)	68	3.4643	0.22	
3.4471	70:	16.8:	H I(1215)	196	3.4469	1.51	
			H I(1025)	66	3.4472	1.12	
			H I(972)	21	(3.4472	2.16)	3
3.4333			H I(1215)	192	3.4330	1.06	
			H I(1025)	64	3.4335	1.31	1,2
			H I(972)	19	3.4339	0.83	2
			H I(949)	4	3.4333	0.72	2
3.3913			H I(1215)	186	3.3913	1.41	
			H I(1025)	54	3.3905	0.66	1
3.3684			H I(1215)	185	3.3684	0.53	
			H I(1025)	50	(3.3701	0.73)	3
3.3569			H I(1215)	182	3.3569	0.53	
			H I(1025)	48	(3.3587	0.96)	3

© American Astronomical Society • Provided by the NASA Astrophysics Data System

© American Astronomical Society • Provided by the NASA Astrophysics Data System

TABLE 4—*Continued*

Adopted redshift	b (km s^{-1})	log N (cm^{-2})	Ident.	Line no.	z_{abs}	W (Å)	Notes*
3.3466			H I(1215)	179	3.3462	0.94	1
			H I(1025)	46	3.3466	0.41	
3.3406	30	15.1	H I(1215)	177	3.3406	0.48	
			H I(1025)	45	3.3411	0.30	
			H I(972)	6	3.3409	0.37	2
3.3223			H I(1215)	172	3.3223	0.76	
			H I(1025)	42	3.3215	0.67	2
3.3073			H I(1215)	167	3.3074	0.67	
			H I(1025)	39	3.3071	0.58	2
3.2872			H I(1215)	163	3.2872	0.84	
			H I(1025)	35	3.2864	0.70	2
3.2603	70	14.4	H I(1215)	159	3.2605	0.61	
			H I(1025)	30	3.2602	0.14	
3.2502			H I(1215)	156	3.2502	0.92	
			H I(1025)	28	(3.2518	0.80)	2
3.2303			H I(1215)	151	3.2306	1.70	4
			H I(1025)	23	3.2301	0.85	1
3.2048			H I(1215)	147	3.2048	1.05	
			H I(1025)	19	(3.2040	0.88)	3
3.1793			H I(1215)	146	(3.18	9.4)	6
			H I(1025)	17	3.1793	0.86	
3.1723			H I(1215)	146	(3.18	9.4)	6
			H I(1025)	16	3.1723	1.53	
3.1463	70	15.1	H I(1215)	141	3.1463	0.96	
			H I(1025)	12	3.1469	0.51	
3.1320			H I(1215)	137	3.1320	0.53	
			H I(1025)	8	(3.1290	1.98)	3
3.1261			H I(1215)	136	3.1261	0.65	
			H I(1025)	8	(3.1290	1.98)	3
3.1215			H I(1215)	135	3.1215	0.68	
			H I(1025)	7	(3.1199	0.92)	3

* NOTES.—(1) Blend with metal line; see text. (2) Some blending obvious from the superposed plots; see text. (3) Identification is a minor (< 50%) but clear contributor to the listed line. (4) Some indication of structure; higher resolution required. (5) Line appears single at this resolution. (6) Included in trough spanning 5060–5116 Å.

1986ApJ...305..496H

TABLE 5

LINE SEARCH LISTS FOR HEAVY-ELEMENT SYSTEMS IN 2000−330

Species	λ_0 (Å)
A. Initial Search List	
C II	1036.34
Fe II	1144.95
Si II	1190.42
Si II	1193.29
Si III	1206.51
Si II	1260.42
O I	1302.17
Si II	1304.37
C II	1334.53
Si IV	1393.76
Si IV	1402.77
B. Supplementary Search List	
H I	920.96
H I	923.15
H I	926.23
H I	930.75
H I	937.80
H I	949.74
H I	972.54
C III	977.03
Si II	989.87
H I	1025.72
O VI	1031.93
O VI	1037.62
O I	1039.23
N II	1083.99
Fe III	1122.53
N I	1134.66(b1)
N I	1199.97(b1)
H I	1215.67
N V	1238.81
N V	1242.80

profiles directly; the plot scales are the same for all species, and the plot widths have been restricted to maintain clarity. The presence of confusing lines shows up clearly in the case of Si II $\lambda\lambda$1190, 1193 at $z_{abs} = 3.1881$, although the numerical entries in Table 6 are highly consistent. The Si III λ1206 profile at $z_{abs} = 3.1914$ appears also to be a blend. There is obvious misalignment of Si III λ1206 at $z_{abs} = 3.1881$ compared with the other species, and this is why its identification remains uncertain.

The Lyβ profile in Figure 5 identifies three main regions of high column density which contribute to the trough at $z_{abs} = 3.18$. No low-ionization heavy-element species can be identified with confidence in the two blueward components from the present Lyα forest data. There is a possibility, however, that they may contain weak C IV (Hunstead *et al.* 1986).

It is of considerable interest to obtain an estimate of the oxygen abundance at such high redshifts. The only O I lines accessible in these systems are $\lambda\lambda$1039, 1302. Unfortunately, each λ1302 line is blended with Lyα in a well-established Lyman-series system (see Table 3); this is not apparent from Figure 5, where the profile match is excellent. Furthermore, only the $z_{abs} = 3.1881$ system shows a λ1039 line without obvious blending. For this system we assume O I to be optically thin and therefore obtain a lower limit of $N(\text{O I}) = 2.4 \times 10^{15}$ cm^{-2}. In Lyα the two systems are completely blended, so we can only determine an upper limit for N(H I) in the 3.1881 system. We do this by assuming Lyα to be fully radiation-damped with equivalent width equal to half that of the broad trough, giving $N(\text{H I}) \leq 4.2 \times 10^{19}$ cm^{-2}. If we assume further that all oxygen exists as O I, we obtain a relative abundance [O/H] $\geq 5.7 \times 10^{-5}$. This should be compared with the solar value of 6.92×10^{-4} (Withbroe 1971). We are led, therefore, to the surprising conclusion that the oxygen abundance at this early epoch is within a factor of 12 of the solar abundance. Indeed, with higher resolution and more realistic estimates of the O and H column densities, it may well be that the oxygen abundance is not substantially different from the $\sim\frac{1}{2}$ solar values seen in the Galactic interstellar medium (York *et al.* 1983).

ii) $z_{abs} = 3.3332$

This system is distinct from the others in 2000−330 in having comparatively weak Lyman lines and possible O VI. The absence of N V, however, and the likely detection of O I may make the O VI detection less plausible.

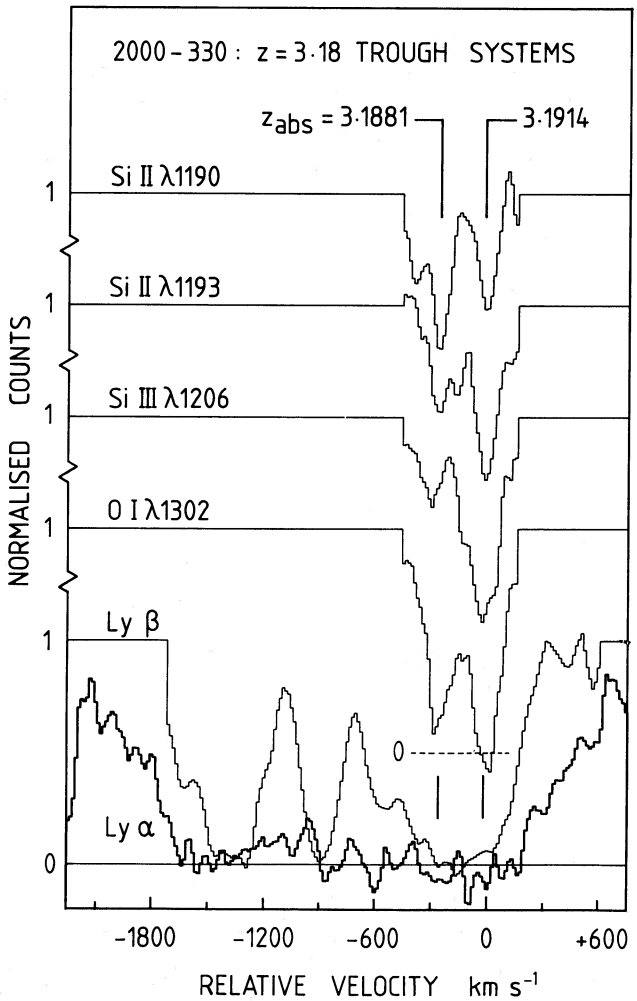

FIG. 5.—Comparison on a common velocity scale of Lyα (*heavier trace*) and Lyβ in the region of the broad trough at $z_{abs} = 3.18$, together with several species detected in the two heavy-element systems. Since these data all fall in the Lyα forest, it is important to recognize the likelihood of blends. The data have been rebinned to 15 km s^{-1} per channel, and the velocity origin is arbitrary. The vertical scale is the same for all species. For the sake of clarity, zero levels have not been shown for the Si lines, and the velocity extent of the regions displayed has been curtailed.

© American Astronomical Society • Provided by the NASA Astrophysics Data System

TABLE 6

HEAVY ELEMENT ABSORPTION SYSTEMS IN 2000−330

Species	λ_o (Å)	Line no.	z_{abs}	W (Å)	f	Comments
z_{abs} = 3.1881 system:						
H I	1215.67	146	3.18:	9.41	0.4162	Broad trough
H I	1025.72	18	3.1888	2.58	0.0791	Blend z=3.1914 system
C II	1334.53	235	3.1877	0.50	0.118	
C II	1036.34	23	3.1868	0.86	0.125	Blend*
N I	1134.66:	...	...	...	0.0804	Not detected
N I	1199.97:	138	3.1888	0.41	0.2657	ID uncertain
N II	1083.99	63	3.1883	0.17	0.101	
O I	1302.17	203	3.1881	0.84	0.0486	Blend*
O I	1039.23	26	3.1881	0.21	0.0092	
Si II	1304.37	205	3.1879	0.26	0.147	
Si II	1260.42	178	3.1884	0.38	0.959	
Si II	1193.28	132	3.1883	0.33	0.500	
Si II	1190.42	130	3.1881	0.31	0.251	
Si III	1206.51	144	3.1874	0.24	1.66	ID uncertain
Si IV	1402.77	...	...	...	0.262	Not detected
Si IV	1393.76	...	...	...	0.528	Not detected
Fe II	1144.95	105	3.1875	0.60	0.15	Blend*
z_{abs} = 3.1914 system:						
H I	1215.67	146	3.18:	9.41	0.4162	Broad trough
H I	1025.72	18	3.1888	2.58	0.0791	Blend z=3.1881 system
C II	1334.53	237	3.1915	0.54	0.118	
C II	1036.34	24	3.1912	0.54	0.125	
N I	1134.66:	98	3.1912	0.86	0.0804	Blend*
N I	1199.97:	139	3.1907	0.45	0.2657	Probable blend
N II	1083.99	64	(3.1951	1.38)	0.101	Blend*
O I	1302.17	204	3.1916	0.85	0.0486	Blend*
O I	1039.23	27	3.1927	0.57	0.0092	Blend*
Si II	1304.37	206	3.1912	0.25	0.147	
Si II	1260.42	179	3.1919	0.97	0.959	Blend*
Si II	1193.28	133	3.1915	0.43	0.500	
Si II	1190.42	131	3.1915	0.25	0.251	
Si III	1206.51	145	3.1913	0.80	1.66	
Si IV	1402.77	...	...	...	0.262	Not detected
Si IV	1393.76	279	3.1913	0.12	0.528	
Fe II	1144.95	106	3.1928	1.22	0.15	Blend*

Species	λ_o (Å)	Line no.	z_{abs}	W (Å)	f	Comments
z_{abs} = 3.3332 system:						
H I	1215.67	175	3.3333	1.14	0.4162	
H I	1025.72	44	(3.3343	2.30)	0.0791	Blend*
H I	972.54	5	(3.3346	1.38)	0.0290	Blend*
C II	1334.53	275	3.3331	0.40	0.118	
C II	1036.34	52	3.3330	0.39	0.125	Blend*
O I	1302.17	249	3.3335	0.25	0.0486	
O I	1039.23	54	(3.3334	0.66)	0.0092	Blend*
O VI	1037.62	53	3.3332	0.53	0.0648	ID uncertain
O VI	1031.93	48	(3.3325	0.97)	0.130	Blend*; ID uncertain
N V	1242.80	...	...	...	0.0757	Not detected
N V	1238.85	...	...	...	0.152	Not detected
Si II	1304.37	251	(3.3322	1.85)	0.147	Blend*
Si II	1260.42	205	(3.3340	0.25)	0.959	Blend*
Si II	1193.28	157	3.3331	0.08	0.500	
Si II	1190.42	154	3.3328	0.28	0.251	Probable blend
Si III	1206.51	165	3.3332	0.57	1.66	
Fe II	1144.95	...	...	...	0.15	Not detected
Fe III	1122.53	114	3.3340	0.13	0.056	ID uncertain
z_{abs} = 3.5519 system:						
H I	1215.67	222	3.5496	3.43	0.4162	See text
H I	1025.72	82	3.5522	1.63	0.0791	
H I	972.54	41	3.5514	1.19	0.02899	
H I	949.74	21	(3.5540	2.11)	0.01394	Blend*
H I	937.80	14	3.5515	0.92	0.00780	
H I	930.75	8	(3.5503	1.80)	0.00481	Blend*
H I	926.23	5	(3.5514	1.32)	0.00318	Blend*
H I	923.15	3	3.5517	0.81	0.00222	
H I	920.96	1	3.5514	1.10:	0.00160	
C II	1036.34	90	3.5521	0.15	0.125	
O I	1039.23	93	3.5515	0.11	0.0092	
Si II	1260.42	267	(3.5528	0.61)	0.959	Blend*
Si II	1193.28	200	3.5515	0.64	0.500	See text
Si II	1190.42	198	3.5517	0.68	0.251	See text
Si II	989.87	55	3.5525	0.63	0.244	Possible blend
Si III	1206.51	212	3.5526	0.44	1.66	
Fe II	1144.95	163	3.5520	0.79	0.15	Blend*

* See Table 3.

© American Astronomical Society • Provided by the NASA Astrophysics Data System

1986ApJ...305..496H

iii) $z_{abs} = 3.5519$

This is the highest redshift heavy-element system seen to date in any QSO, and it is the system responsible for the continuum cutoff below 4200 Å. The Lyman limit in this system falls at 4150 Å, but the crowding of higher order Lyman lines causes the apparent cutoff to be shifted redward. It is evident from the redshifts in Table 6 and from superposed plots of the Lyman lines that the high column density cloud producing the continuum cutoff is offset from the centroid of the Lyα profile; a similar situation was noticed for the systems near $z_{abs} = 3.19$. This suggests a local aggregation of clouds or maybe a cluster, the total span in velocity here being ~ 900 km s^{-1}.

The Si II identifications in this system (Table 6) appear plausible based on their wavelength match, while the similar line strengths are consistent with the Si II lines falling on the flat portion of the curve of growth. However, line 267, which is identified here as Si II λ1260, has an alternative identification as Lyα in a clear Lyman-series system at $z_{abs} = 3.7203$ (Table 4). Since λ1260 is the strongest Si II transition, this implies that the other three Si II lines must also be blends and that the good wavelength match is probably fortuitous. A superposed plot confirms this interpretation, although it is difficult to quantify the amount of blending in each case. The lesson is clear: when seeking line identifications in the Lyα forest, it is *not* sufficient to rely on wavelength matching alone—it is essential to examine line profiles as well.

Additional information about this system comes from recent spectra obtained redward of Lyα emission. In particular, Si IV λλ1393, 1402 is strong with good evidence for velocity structure (Hunstead *et al.* 1986). Preliminary measures for the dominant Si IV component are given in Table 7. The redshift of this component is slightly greater than the adopted system redshift, which we attribute to blending with the blueward components (Hunstead *et al.* 1986, Fig. 1), notably in H I (see Table 6). A more detailed investigation of the velocity structure of Si II, Si IV, C II, and C IV in this system is currently in progress.

TABLE 7

PRELIMINARY MEASURES FOR Si IV IN THE $z_{abs} = 3.55$ SYSTEM

Line	λ[a] (Å)	z_{abs}	W_{obs} (Å)
Si IV λ1393.755.....	6344.80	3.55230	1.00
Si IV λ1402.770.....	6385.84	3.55230	0.57

[a] Wavelengths are vacuum, heliocentric values.

VI. SUMMARY

1. The absorption spectrum of 2000−330 is characterized by an extremely high density of lines blueward of Lyα emission. This created difficulties first in setting continuum levels and thereafter in defining suitable boundaries between partially blended lines. In general we have counted features with broad or slightly asymmetric profiles as single.

2. Asymmetry in the observed profile of Lyα emission can plausibly be explained by Si III λ1206 emission. This line has not previously been seen in emission in a QSO.

3. The mean density of Lyα absorption lines in 2000−330 has been compared with the corresponding values obtained by Young, Sargent, and Boksenberg (1982) at lower redshift. Adopting their selection criteria we find an increase in line density of 3.3 σ for $q_0 = 0$ and 4.3 σ for $q_0 = \frac{1}{2}$ between $\langle z \rangle = 1.83$ and 3.41. This provides very firm evidence for evolution in the number density of hydrogen clouds responsible for the Lyα absorption forest.

4. A thorough search has been made for Lyman-series and heavy-element absorption systems. This search covered the range $3.10 < z_{abs} < 3.78$ and yielded 45 Lyman systems and four heavy-element systems. The plausibility of these systems was assessed using superposed plots of the various transitions/species on logarithmic wavelength scales. This technique allowed both alignments and relative strengths to be readily examined and drew attention to deficiencies in conventional methods based solely on wavelength matching.

5. The system at $z_{abs} = 3.5519$ is the highest redshift heavy-element system seen to date in any QSO and is responsible for the continuum cutoff below 4200 Å. The ionization structure is similar to that seen in other QSO absorption systems at lower redshift. On the other hand, the system at $z_{abs} = 3.1881$ is unusual in being exclusively a low-ionization system with no detectable Si IV or C IV. In this system we estimate $[O/H] \geq -1.1$ dex relative to solar, based on weak O I λ1039 and blended Lyα. With higher resolution and more realistic estimates of N(O I) and N(H I), it may well be that the oxygen abundance at this early epoch is not substantially different from the $\sim \frac{1}{2}$ solar abundance seen in the Galactic interstellar medium.

We thank John Straede for assistance with the AAO reduction software and the AAT mountain staff for assistance with the observations. R. W. H. and H. S. M. acknowledge support from the Australian Research Grants Scheme.

REFERENCES

Bahcall, J. N. 1968, *Ap. J.*, **153**, 679.
Carswell, R. F., Morton, D. C., Smith, M. G., Stockton, A. N., Turnshek, D. A., and Weymann, R. J. 1984, *Ap. J.*, **278**, 486.
Carswell, R. F., Whelan, J. A. J., Smith, M. G., Boksenberg, A., and Tytler, D. 1982, *M.N.R.A.S.*, **198**, 91.
Hunstead, R. W., Murdoch, H. S., Pettini, M., and Blades, J. C. 1986, *Ap. Space Sci.*, in press.
Jauncey, D. L., Batty, M. J., Gulkis, S., and Savage, A. 1982, *A.J.*, **87**, 763.
Morton, D. C. 1978, *Ap. J.*, **222**, 863.
Murdoch, H. S., Hunstead, R. W., Pettini, M., and Blades, J. C. 1985, *Ap. J.*, submitted (Paper II).
Oke, J. B. 1974, *Ap. J. Suppl.*, **27**, 21.
Osmer, P. S. 1983, in *IAU Symposium 104, Early Evolution of the Universe and Its Present Structure*, ed. G. O. Abell and G. Chincarini (Dordrecht: Reidel), p. 35.
Peterson, B. A. 1983*a*, in *IAU Symposium 104, Early Evolution of the Universe and Its Present Structure*, ed. G. O. Abell and G. Chincarini (Dordrecht: Reidel), p. 349.
———. 1983*b*, in *Quasars and Gravitational Lenses, Proc. 24th Liège Astrophysical Colloquium*, p. 563.
Peterson, B. A., Savage, A., Jauncey, D. L., and Wright, A. E. 1982, *Ap. J. (Letters)*, **260**, L27.

© American Astronomical Society • Provided by the NASA Astrophysics Data System

1986ApJ...305..496H

Withbroe, G. L. 1971, *The Menzel Symposium*, ed. K. B. Gebbie (NBS Spec. Pub.), p. 353.
York, D. G., Spitzer, L., Bohlin, R. C., Hill, J., Jenkins, E. B., Savage, B. D., and Snow, T. P. 1983, *Ap. J. (Letters)*, **266**, L55.
Young, P. J., Sargent, W. L. W., and Boksenberg, A. 1982, *Ap. J.*, **252**, 10.
Young, P. J., Sargent, W. L. W., Boksenberg, A., Carswell, R. F., and Whelan, J. A. J. 1979, *Ap. J.*, **229**, 891.

J. C. BLADES: Space Telescope Science Institute, 3700 San Martin Drive, Homewood Campus, Baltimore, MD 21218

R. W. HUNSTEAD and H. S. MURDOCH: School of Physics, University of Sydney, N.S.W. 2006, Australia

D. L. JAUNCEY: CSIRO Division of Soils, P.O. Box 639, Canberra, A.C.T. 2601, Australia

B. A. PETERSON: Mount Stromlo Observatory, Private Bag, Woden P.O., A.C.T. 2606, Australia

M. PETTINI: Royal Greenwich Observatory, Herstmonceux Castle, Hailsham, East Sussex BN27 1RP, England

A. SAVAGE: Royal Observatory, Blackford Hill, Edinburgh EH9 3HJ, Scotland

A. E. WRIGHT: CSIRO Division of Radiophysics, P.O. Box 276, Parkes, N.S.W. 2870, Australia

© American Astronomical Society • Provided by the NASA Astrophysics Data System